bioRxiv preprint doi: https://doi.org/10.1101/2021.08.26.457824; this version posted August 28, 2021. The copyright holder for this preprint (which was not certified by peer review) is the author/funder, who has granted bioRxiv a license to display the preprint in perpetuity. It is made available under aCC-BY-NC-ND 4.0 International license.

Title: A Multi-Omics Human Liver Organoid Screening Platform for DILI Risk Prediction

Authors: Charles J. Zhang[1], Matthew J. O'Meara[2], Sophia R. Meyer[1], Sha Huang[3], Meghan M. Capeling[3], Daysha Ferrer-Torres[3], Charlie J. Childs[4], Jason R. Spence[3,4], Robert J. Fontana[3]*, Jonathan Z. Sexton[1,3,5]*

Affiliations:

[1]Department of Medicinal Chemistry, College of Pharmacy, University of Michigan, Ann Arbor, MI, 48109, USA
[2]Department of Computational Medicine and Bioinformatics, University of Michigan, Ann Arbor, MI, 48109, USA
[3]Department of Internal Medicine, Gastroenterology and Hepatology, Michigan Medicine at the University of Michigan, Ann Arbor, MI, 48109, USA.
[4]Department of Cell and Developmental Biology, University of Michigan, Ann Arbor, MI, 48109, USA.
[5]U-M Center for Drug Repurposing, University of Michigan, Ann Arbor, MI, 48109, USA
*Corresponding author jzsexton@med.umich.edu

ORCID IDs:

CJZ: 0000-0003-0300-849X
MJO: 0000-0002-3128-5331
SRM: 0000-0002-7301-8370
SH: NA
MMC: 0000-0003-0310-123X
DFT: 0000-0002-3576-0347
CJC: 0000-0002-4480-2625
JRS: 0000-0001-7869-3992
RJF: 0000-0001-9161-5892
JZS: 0000-0002-9244-5888

Classification: Biological Sciences - Medical Sciences

Keywords: DILI, microfluidic devices screening, liver organoids

Abbreviations:

DILI: drug-induced liver injury

ALT: alanine aminotransferase

HLO: human liver organoid

bioRxiv preprint doi: https://doi.org/10.1101/2021.08.26.457824; this version posted August 28, 2021. The copyright holder for this preprint (which was not certified by peer review) is the author/funder, who has granted bioRxiv a license to display the preprint in perpetuity. It is made available under aCC-BY-NC-ND 4.0 International license.

iPSC: induced-pluripotent stem cells

HLA: human leukocyte antigen

PaDLOC: patient-derived liver-on-chip

scRNAseq: Single cell RNA sequencing

Conflicts of interest: The authors declare no conflicts of interest.

Abstract

Background and Aims

Drug-induced liver injury (DILI) is a prominent failure mode in drug development resulting in clinical trial failures and post-approval withdrawal. Improved in vitro models for DILI risk prediction that can model diverse genetics are needed to improve safety and reduce high attrition rates in drug development. In this study, we evaluated the utility of human liver organoids (HLOs) for high-throughput DILI risk prediction and in an organ-on-chip system. The recent clinical failure of inarigivir soproxil due to DILI underscores the need for improved models.

Methods

HLOs were adapted for high-throughput drug screening in dispersed-cell 384-well format and a collection of DILI-associated drugs were screened. HLOs were also adapted to a liver-chip system to investigate enhanced *in vivo*-like function. Both platforms were benchmarked for their ability to predict DILI using combined biochemical assays, microscopy-based morphological profiling, and transcriptomics.

Results

bioRxiv preprint doi: https://doi.org/10.1101/2021.08.26.457824; this version posted August 28, 2021. The copyright holder for this preprint (which was not certified by peer review) is the author/funder, who has granted bioRxiv a license to display the preprint in perpetuity. It is made available under aCC-BY-NC-ND 4.0 International license.

Dispersed HLOs retained DILI predictive capacity of intact HLOs and are amenable to high-throughput screening allowing for measurable IC_{50} values for cytotoxicity. Distinct morphological differences were observed in cells treated with drugs exerting differing mechanisms of action. HLOs on chips were shown to increase albumin production, CYP450 expression and also release ALT/AST when treated with known DILI drugs. Importantly, HLO liver chips were able to predict hepatotoxicity of tenofovir-inarigivir and showed steatosis and mitochondrial perturbation via phenotypic and transcriptomic analysis.

Conclusions

The high throughput and liver-on-chip system exhibit enhanced *in vivo*-like function and demonstrate the utility of the platforms in early and late-stage drug development. Tenofovir-inarigivr associated hepatotoxicity was observed and highly correlates with the clinical manifestation of DILI.

Introduction

Drug-induced liver injury (DILI) is an infrequent but important cause of both acute and chronic liver disease.[1,2] An estimated 22% of clinical trial failures and 32% of market withdrawals of therapeutics are due to hepatotoxicity, highlighting the role of the liver as a significant site of adverse drug reactions leading to drug failure.[3,4] This potential hepatotoxicity creates an increased risk for clinical trial participants as well as a financial burden in drug development. Hepatotoxicity is usually not detected in preclinical or clinical studies but instead is observed only in the clinic or post-marketing settings. These toxicities are termed “idiosyncratic,” since they are largely independent of the dose and duration of drug use and develop in only a small proportion of treated patients for as-yet unclear reasons. As there are currently over 1000 prescription medications and >100,000 herbal and dietary supplements (HDS) available for use in the United States, with 45% of all

bioRxiv preprint doi: https://doi.org/10.1101/2021.08.26.457824; this version posted August 28, 2021. The copyright holder for this preprint (which was not certified by peer review) is the author/funder, who has granted bioRxiv a license to display the preprint in perpetuity. It is made available under aCC-BY-NC-ND 4.0 International license.

Americans reported taking at least one prescription medication in the past month and 11% reported taking more than 5 prescriptions[5], the potential for synergistic liver toxicity is high.

Recently, Spring Bank Pharmaceuticals was investigating inarigivir soproxil (GS-9992), an oral immunomodulator that inhibits retinoic acid-inducible gene I (RIG-I) protein leading to enhanced intracellular IFN signaling pathways against Hepatitis B (HBV).[6] Inarigivir monotherapy and in combination with tenofovir alafenamide (TAF) was evaluated at a daily dose of 25 to 900 mg and showed no clear signs of toxicity in two clinical trials for HBV; a phase-1 monotherapy study in non-cirrhotic, treatment-naive subjects with HBV (NCT04059198) and a phase-2 study of inarigivir/TAF in chronic HBV subjects (NCT03434353). However, a phase-2 inarigivir/TAF study identified severe DILI in 7 of 42 patients given the combination of both drugs after 16 weeks of therapy, thus leading to the halt of the phase-2 trial. All 7 patients had an elevated alanine aminotransferease (ALT) after 16 weeks of therapy, 4 of the 7 had associated hyperbilirubinemia, and one subject died due to multiorgan system failure with lactic acidosis and evidence of hepatic steatosis in their liver suggestive of possible mitochondrial toxicity.[7]

This clinical trial failure underscores the need for high fidelity pre-clinical DILI risk prediction. The challenge in determining DILI risk assessment arises from the lack of pre-clinical systems that model the physiologic functions of the human liver. Common *in vitro* models include hepatocellular carcinoma-derived cell lines (HepG2, Huh7, HepaRG, etc.), which do not recapitulate hepatocyte function and assume that DILI is a hepatocyte-cell autonomous effect.[8] An alternative is primary human hepatocyte (PHH) cell cultures, which retain hepatocyte function but whose metabolic function declines rapidly and varies greatly between cadaveric fresh and cryopreserved samples.[9] PHH cultures are also costly to scale for the high-throughput screening necessary to enable large-scale screening for DILI-risk.[10] Modeling human liver injury in laboratory animals is

bioRxiv preprint doi: https://doi.org/10.1101/2021.08.26.457824; this version posted August 28, 2021. The copyright holder for this preprint (which was not certified by peer review) is the author/funder, who has granted bioRxiv a license to display the preprint in perpetuity. It is made available under aCC-BY-NC-ND 4.0 International license.

also not scalable and often proves inadequate due to species differences between humans, dogs, and rodents and an overall lack of mechanistic understanding of idiosyncratic DILI.[11,12]

To meet this challenge, we explored the use of human liver organoids (HLO) as a more physiologically organotypic system for recapitulating DILI in vitro, with added adaptations for high-throughput screening. We started with a previously-developed protocol for derivation of human liver organoids from induced pluripotent stem cells (iPSC) and adapted their use for high-throughput drug screening in both 384-well plates and in a liver-chip system for enhanced physiological fidelity.[13] HLOs consist primarily of hepatocytes but also include non-parenchymal stellate and Kupffer cells, and all of the cells arise from the same individual donor.[14] In this study, we adapted the HLOs for high-throughput screening and an organ-on-chip system (Emulate Bio)[15] to compare and contrast specific endpoints, including iPSC-hepatocyte maturity and drug responsiveness, across the two platforms. Liver chips have been previously used to successfully predict species-specific DILI in primary hepatocytes;[12] by validating the iPSC-derived liver organoid chip system, we would then be able to assess patient-specific DILI.

Due to the complexity of DILI, we developed an integrated multi-omics platform including biomarker/analyte detection, phenotyping of the cell population with high content imaging, and single-cell RNA sequencing to deliver a comprehensive platform for dissection of DILI mechanisms and to enable personalized DILI risk prediction. In this study, we performed scRNA sequencing transcriptomics and morphological cell profiling to supplement the liver chip endpoints to suggest a possible mechanism of action of tenofovir-inarigivir hepatotoxicity. Our efforts have demonstrated the potential of dispersed HLOs for rapid 384-well based compound DILI-risk screening, and also the validation of a patient-derived liver-on-chip (PaDLOC) system for a more intricate, but lower throughput, model for DILI.

bioRxiv preprint doi: https://doi.org/10.1101/2021.08.26.457824; this version posted August 28, 2021. The copyright holder for this preprint (which was not certified by peer review) is the author/funder, who has granted bioRxiv a license to display the preprint in perpetuity. It is made available under aCC-BY-NC-ND 4.0 International license.

Materials and Methods

Human liver organoid culture and dispersion

Human iPSC line 72.3 was obtained from Cincinnati Children's Hospital Medical Center[16] and differentiated into HLOs based on a previously described protocol.[13,14] In brief, iPSCs were grown to 90% confluency on Matrigel (Corning, 354234) in 6-well plates. Cells were then treated with Activin A (R&D Biosystems, 338-AC) for 3 days and FGF4 (purified in house[17]) for 3 additional days to form definitive endoderm spheroids. Spheroids were embedded in Matrigel and treated with retinoic acid for 4 days followed by Hepatocyte Culture Medium BulletKit (Lonza, CC-3198) supplemented with hepatocyte growth factor (PeproTech, 100-39) for 12 days.

HLOs were then taken out of Matrigel by treatment with dispase (0.2 mg/mL) for 10 minutes and washed with DMEM/F12 (ThermoScientific, 11320033) with centrifugation at 300 x g for 3 minutes to pellet between washes. To achieve a single cell suspension, cells were treated with trypsin (0.25%) (Invitrogen, 25200056) and incubated at 37 ºC for 10 minutes, mechanically dissociated by pipetting, and incubation for an additional 10 minutes. Trypsin was quenched with 100% FBS and washed 3 times with DMEM/F12.

PaDLOC Culture and Compound Treatment

Dispersed cells were transferred to the Chip S1™ based on the co-culture Liver-Chip Culture Protocol as described by Emulate Bio.[18] In brief, both channels of the S1 are first activated with the manufacturer's ER-1 solution and UV treatment. Activated chips are then washed with cold PBS (ThermoFisher Scientific, 10010023) and both channels were coated with an extracellular matrix consisting of collagen I (100 µg/mL)

bioRxiv preprint doi: https://doi.org/10.1101/2021.08.26.457824; this version posted August 28, 2021. The copyright holder for this preprint (which was not certified by peer review) is the author/funder, who has granted bioRxiv a license to display the preprint in perpetuity. It is made available under aCC-BY-NC-ND 4.0 International license.

(Corning, 354249) and fibronectin (25 µg/mL) (ThermoScientific, 33010018) at 4 ºC overnight followed by 1 hr at 37 ºC.

Extracellular matrix coating was then washed off with hepatocyte growth media before use. Dispersed HLOs were concentrated to a density of 4 x 10^6 cells/mL. 50 µL of cell suspension was quickly pipetted into the top channel to allow even dispersion and cultured static (no media flow) at 37 ºC for 8 hrs for attachment to the semi-permeable membrane. Next, 30 µL of cell suspension was seeded into the bottom channel and the chip immediately flipped over to allow attachment to the membrane, on the bottom layer. Again, cells were left to attach for 8 hrs at 37 ºC. Both channels were then gravity washed with hepatocyte growth media de-gassed with a 0.45 µm Steriflip-HV Sterile Centrifuge Tube Top Filter Unit (MilliporeSigma, SE1M003M00).

Each seeded Chip S1 was then attached to a respective Pod™ Portable Module. De-gassed hepatocyte growth media was used to fill the inlet reservoirs for both the top and bottom channels. Loaded Pods were then placed into the Zoë™ Culture Module at 37 ºC. All chips then underwent a regulate cycle followed by a constant flow rate of 30 µL/hr of the reservoir's media for each of both channels. Flow is modulated by an Orb™ Hub Module. Media outflow collected in respective reservoirs was obtained for albumin, ALT, AST, and LDH quantification. Fresh de-gassed hepatocyte growth media was added into the inlet reservoirs every 2 days. Cells were cultured on this system for 7 days before treatments.

After 7 days, residual hepatocyte growth media was aspirated and replaced with hepatocyte growth factor containing either 0.1% DMSO, APAP (100 µM), FIAU (1 µM), tenofovir (500 nM), inarigivir soproxil (500 nM), or tenofovir and inarigivir soproxil (250 nM and 250 nM). The flow rate was maintained as prior for an additional 7 days and outflow media was collected pre-treatment and days 1, 3, and 7 for albumin, ALT, AST, and LDH quantification.

bioRxiv preprint doi: https://doi.org/10.1101/2021.08.26.457824; this version posted August 28, 2021. The copyright holder for this preprint (which was not certified by peer review) is the author/funder, who has granted bioRxiv a license to display the preprint in perpetuity. It is made available under aCC-BY-NC-ND 4.0 International license.

Dispersed 384-well HLO culture and drug delivery

Dispersed HLOs were seeded in collagen type 1-coated CellCarrier-384 Ultra Microplates (PerkinElmer, 6057308) at a seeding density of 8,000 cells/well in hepatocyte growth media. Cells were left to adhere and culture for 48 hrs before treatment with compounds. For screening, compounds were dispensed in 10-point dose-response from 2 nM to 500 μM using an HP D300e Digital Dispenser. For tenofovir-inarigivir synergy assessment, tenofovir, inarigivir sorpoxil, and in combination were dispensed in triplicate with 12-point dose-response curves in 1/3 dilutions starting with a high of 500 μM. Cells were then incubated for 72-hours before fixation and staining.

Single-cell transcriptomics

Single-cell RNA sequencing was performed on dispersed HLOs and PadLOCs using the Illumina NovaSeq platform for vehicle controls and cells treated with fialuridine, tenofovir, and tenofovir-inarigivir in combination. Each sample generated between 440 and 860 million barcoded reads corresponding to an estimated 4,600 to 25,000 cells per sample (SI scRNAseq_metric_summary.xls). Transcripts were mapped to the GRCh38 2020-A (GENCODE v32/Ensembl 98) (July 7th, 2020) reference transcriptome[19] using 10x Genomics Cell Ranger 5.0.1,[20] where between 45% and 58% of reads per sample confidently map to the transcriptome, yielding between 500 and 4,700 median genes per cell. As a quality filter, genes were excluded if they were only detected in 5 or fewer cells, and cells were excluded if over 30% of reads were mitochondrial or if they had fewer than 10,000 total reads. Except for inarigivir, where only 170 cells passed quality control, between 1,700 and 4,400 cells were retained for each sample. Given that hepatocytes may be binucleated,[21] we did not remove doublets.

bioRxiv preprint doi: https://doi.org/10.1101/2021.08.26.457824; this version posted August 28, 2021. The copyright holder for this preprint (which was not certified by peer review) is the author/funder, who has granted bioRxiv a license to display the preprint in perpetuity. It is made available under aCC-BY-NC-ND 4.0 International license.

To estimate differential expression, we first correct for over-dispersion using sctransform v2 [22] with Seurat v4[23] which fits a robust negative binomial model for the per-gene variance by the expression mean. We then used DESeq2 to compute the average log fold-change and adjusted p-value for each gene between cells under different conditions.[24]

To visualize and cluster cells with distinct phenotypes, we used UMAP non-linear dimensionality reduction[25] in monocle3.[26] Expression values were normalized by dividing by per-cell size factors, adding a pseudo-count of 1, and taking the natural log; reducing the dimensionality with principal component analysis to 100 dimensions; and then applying the UMAP algorithm implemented in uwot[27] using the monocle3 default arguments: similarity="cosine", min_dist=0.1, n_neighbors=15. To estimate clusters, we applied the Leiden modularity algorithm[28] to the gene UMAP coordinates setting the resolution of $1e^{-4}$ when embedding the untreated PaDLOC and HLO samples, and a resolution of 1e-5 when embedding the PaDLOC samples and default parameters otherwise.

Image Acquisition

384-well cultures and intact organoids (transferred to 384-well plates) were imaged on a Yokogawa CellVoyager 8000 High-Content Screening System and maximum intensity projection images were acquired for with 1µm Z-spacing and 15 µm depth. PaDLOCs were imaged with a Yokogawa CQ1 Benchtop High-Content Analysis System with 1 µm sections through 100 µm with both upper and lower chip compartments imageable.

Cell Morphological Profiling and Data Analysis

Multi-channel fluorescence images were analyzed with CellProfiler 4.2.0. Individual nuclei were first identified using Otsu thresholding and segmentation. The entire cell was delineated using the nucleus as a seed object and

bioRxiv preprint doi: https://doi.org/10.1101/2021.08.26.457824; this version posted August 28, 2021. The copyright holder for this preprint (which was not certified by peer review) is the author/funder, who has granted bioRxiv a license to display the preprint in perpetuity. It is made available under aCC-BY-NC-ND 4.0 International license.

dilation to the extent of the cell boundary and enabled measurements of fluorescent intensity, intensity distribution, texture, size, and shape from the respective regions in each fluorescent channel. For 384-well biomarker immunofluorescence assays, cells were stained with Hoechst 33342 (ThermoFisher Scientific, H3570), CEBPA (MilliporeSigma, HPA052734), VIM (ThermoFisher Scientific, 14989782), and CD68 (Abcam, ab53444) or with Hoechst 33342, ASGR1 (ThermoFisher Scientific, MA140244) and αSMA (Abcam, ab21027). For 384-well hepatotoxicity assays, plates were stained with Hoechst 33342, MitoView Green (Biotium, 70054), HCS CellMask Orange(ThermoFisher Scientific, H32713), and HCS LipidTox Deep Red (ThermoFisher Scientific, H34477). PaDLOCs were stained with Hoechst 33342, HCS CellMask Orange, and HCS LipidTox Deep Red.

The resulting data set includes hundreds of measurements on a per-cell level with necessary metadata relating each cell to their respective field, well, and plate. Cell viability across compound dose-range was obtained based on the number of identified cells per condition with the DMSO vehicle-treated control as the 100% viability reference. For UMAP-embedding, measurements for each feature were centered at zero and scaled with Z-score=1. Features with low variance were omitted. UMAP embedding was done with the Python umap-learn package.[29]

Random forest model training and prediction were done with KNIME.[30,31] In brief, the cell-feature matrix was centered/scaled and low variance features were omitted and highly correlated features (>95%) were also omitted. Data was then split into training and test sets with an 80/20 split and model performance were evaluated on the test set and the model was found to have an accuracy of >90%. After training/testing, the model was deployed to score the entire dataset.

bioRxiv preprint doi: https://doi.org/10.1101/2021.08.26.457824; this version posted August 28, 2021. The copyright holder for this preprint (which was not certified by peer review) is the author/funder, who has granted bioRxiv a license to display the preprint in perpetuity. It is made available under aCC-BY-NC-ND 4.0 International license.

Results

Use of Dispersed HLOs in 384-well Based High-Content Screening

We generated HLOs from iPSC line 72.3 by culturing iPSCs to definitive endoderm spheroids through a 6-day differentiation.[14,32] Spheroids were then embedded into Matrigel (Corning, 354234) and cultured in media containing hepatocyte growth factor for 15 additional days (Figure 1A). 3D confocal immunofluorescence imaging was then performed to verify the presence of liver-specific cell types, using Hoechst 33342 to stain for nuclei, anti-CEBPA, and anti-ASGR1 to identify hepatocytes, VIM, and αSMA to identify stellate cells, and CD68 to identify Kupffer cells (Figure 1B). Hepatic stellate cells and Kupffer cells are well established in the etiology of liver injury from inflammatory stress[33] and the concomitant development of fibrosis.[34]

Intact HLOs have been shown to recapitulate cytotoxicity of known hepatotoxic drugs.[35] However, the scalability of 3D HLOs for drug screening is not optimal and translation to high-throughput screening is a significant challenge. Dispersing HLOs into 384-well monolayer cultures allows for homogenous drug exposure, homogenous cell-type distribution, and morphologic characterization and adaptation for high content screening in 384-well format.[36] Although we have been able to disperse iPSC-based organoids into 384-well plate cultures and observed retention of tissue-specific markers and function,[37] loss of cell identity (de-differentiate) and organotypic responsiveness to drugs was of concern. Here, we dispensed 3,500 dispersed HLO cells/well in 384-well plates and observed slow proliferation across 7-days (Supplementary Figure 1A) while they retained cell-type-specific markers, albumin production, and CYP 450 expression (Figure 2A, Supplementary Figure 1 B-C) at day 7 of culture. This indicates that they retain physiologic functions in the dispersed state. CellProfiler 4.2.0[38] was used to segment cells using nuclei staining and measure the intensity and distribution of each marker on a per-cell level to check for marker positivity. 59.7% were positive for

bioRxiv preprint doi: https://doi.org/10.1101/2021.08.26.457824; this version posted August 28, 2021. The copyright holder for this preprint (which was not certified by peer review) is the author/funder, who has granted bioRxiv a license to display the preprint in perpetuity. It is made available under aCC-BY-NC-ND 4.0 International license.

CEBPA, 35.6% for VIM, 0.19% for CD68 and 4.58% for neither (Supplementary Figure 1A-B). These cell ratios match previously determined cell distribution through scRNAseq.[14]

To test the feasibility of using these dispersed HLOs as a DILI screening platform, we performed assay development and screened a collection of DILI-associated drugs and probes that produce liver toxicity in other systems. Compounds were tested in 10-point/2-fold dilution concentration-response format in optical-bottom 384-well plates with fialuridine (FIAU) as a positive control and DMSO vehicle control. We measured cell viability by reductions in cell counts (relative to the vehicle control) and morphological perturbation as a tool to classify compounds by their phenotypic signature and to impute their mechanism of action by similarity to compounds with known mechanisms of action. 12 compounds showed clear dose-responsive loss of cell viability with IC_{50} values between 150 nM - 31.4 μM. Huh7 and dispersed definitive endoderm were counter-screened in the same manner and neither exhibited overt cytotoxicity (Figure 2B), establishing that HLOs exhibit hepatocyte-specific metabolism and response to drugs.

Morphologic profiling of DILI compound effects in dispersed 384-well culture.

To characterize the drug-induced perturbation of single-cells in response to 12 hepatotoxic drugs from 384-well plate screening, we used CellProfiler 4.2.0 to segment and extract 845 features per cell to generate a cell-by-feature matrix. The dimensionality of the feature vector was reduced to 2-dimensions using the uniform manifold approximation and projection (UMAP) method[29] and hierarchical density-based clustering was performed with HDBScan[39] to characterize and cluster drug treatments by their resulting phenotypic perturbation. We observe three distinct clusters within this embedding (Figure 2C, Supplementary Figure 2). Cluster α consists largely of allopurinol, tamoxifen, and thioguanine-treated cells, all thought to cause DILI through an immunological response to their metabolites. Cluster β contains cells treated with

bioRxiv preprint doi: https://doi.org/10.1101/2021.08.26.457824; this version posted August 28, 2021. The copyright holder for this preprint (which was not certified by peer review) is the author/funder, who has granted bioRxiv a license to display the preprint in perpetuity. It is made available under aCC-BY-NC-ND 4.0 International license.

nucleotide/nucleoside analogs and consists mainly of cells treated with propylthiouracil, and to a lesser extent, stavudine, and thioguanine-treated cells. Lastly, Cluster γ contains a majority of cells treated with allopurinol and tamoxifen as in Cluster β, but with a major presence of nevirapine and rifampin which are thought to cause DILI through CYP450 modulation. With other compounds, less pronounced clustering was observed (Supplementary Figure 2).

Biochemical, phenotypic, and transcriptomic analysis of HLOs in an Organ-on-a-Chip System - iPSC Liver Chips

At day 21 of differentiation, HLOs were dispersed into a single-cell suspension and seeded in both upper and lower compartments of a dual-compartment microfluidic S1 chip (Emulate Bio), and cultured for an additional 7 days to develop a patient-derived liver-on-chip (PaDLOC). The dual-compartment microfluidic S1 chip was previously used for long-term culture and maintenance of primary hepatocytes[40]. Primary hepatocytes on this system were shown to respond to DILI-causing compounds and recapitulate species-specific toxicity over the current preclinical standard models.[12]

First, while intact HLOs were shown to produce 6.74 μg/mL albumin per 10^6 cells with slight diminishment after 7 days of culture, PaDLOCs released more albumin to a rate of 30.9 ug/mL per 10^6 cells (Figure 3A). This is comparable to albumin production by primary hepatocytes cultured on the same chip system.[11] PaDLOCs also express CYPs 1A1, 2D6, and 3A4 at 4-5 fold higher levels as compared to intact HLOs and 100-fold higher levels than immortalized liver cell lines Huh7 or Ph5 (Figure 3B). Lastly, PaDLOCs exposed to media containing BSA-conjugated oleate were shown to accumulate lipid, producing a steatotic state (Supplementary Figure 4).

bioRxiv preprint doi: https://doi.org/10.1101/2021.08.26.457824; this version posted August 28, 2021. The copyright holder for this preprint (which was not certified by peer review) is the author/funder, who has granted bioRxiv a license to display the preprint in perpetuity. It is made available under aCC-BY-NC-ND 4.0 International license.

scRNA sequencing of HLO cells was performed using the Illumina NovaSeq platform to confirm the presence of hepatocytes in both PaDLOCs and HLOs, and also to compare the transcriptomic changes imparted by the on-chip culture system. Single-cell analysis was performed for comparisons of culture conditions (Figure 3G). A general increase in hepatocyte maturity/function was observed in PaDLOCs relative to HLOs. Differential expression analysis between all cells of HLO and PaDLOCs (Figure 3H) showed an increase of TGFBI (collagen binding) and CCN2 expression (cell adhesion) in PaDLOCs that are biomarkers of liver proliferation.[41] We also observed an increased expression of cytokine response/signaling, and corticosteroid response markers. Increased expression of hepatocyte-marker TDO2 was observed and is commonly correlated with increased CYPs 1A1 and 1A2[42] and ACTA2, a marker for activated stellate cells.[43] Other liver-specific markers demonstrating increased expression in PaDLOCs include NNMT,[44] and IGFBP7.[45] Enrichment analysis suggests an upregulation of cell structural components such as actin cytoskeleton organization, actin filament-based processes, and cytoskeleton organization. Enrichment also shows a general increase in inflammatory response elements (Supplementary Figure 5) (scRNAseq data is available at GEO).

iPSC liver chips for DILI risk prediction

Serum biomarkers for DILI include elevated ALT/AST[46] and diminished production of albumin.[47] These biomarkers correspond to hepatocellular injury and can be assayed similarly in liver-chip media effluent with acetaminophen (APAP) and filauridine (FIAU) as positive controls with differing mechanisms of action. APAP is metabolized by CYP450-mediated oxidation to NAPQI that exerts hepatotoxicity via the formation of covalent liver protein adducts at cysteine residues as 3-(cystein-*S*-yl)-APAP.[48,49] FIAU also causes hepatotoxicity by stimulating ectopic lipid accumulation and as a mitochondrial toxin.[50,51] From exposure to 100 μM of APAP, ALT increased from a basal level of 8 U/L at day 0 to a peak of 22 U/L at day 4 and a seeming recovery by day 7 with a reduction in both ALT and AST release (Figure 3C and D). Treatment with

bioRxiv preprint doi: https://doi.org/10.1101/2021.08.26.457824; this version posted August 28, 2021. The copyright holder for this preprint (which was not certified by peer review) is the author/funder, who has granted bioRxiv a license to display the preprint in perpetuity. It is made available under aCC-BY-NC-ND 4.0 International license.

10 μM FIAU resulted in a drastic increase to over 80 U/L for both ALT and AST at 7-days after exposure with no indication of recovery in this period. Additionally, albumin production, a guiding biomarker for the diagnosis of DILI severity,[47] was stable in DMSO-treated PaDLOCs while its production was diminished in both APAP and FIAU-treated PaDLOCs (Figure 3E).

Importantly, DILI from APAP and FIAU manifest differently in the liver to differing mechanisms of action. The multifaceted nature of DILI-causing drugs presents a challenge for DILI-risk prediction for novel therapeutics. For example, APAP has been reported to cause hepatic necrosis[52] whereas FIAU causes diffuse microvesicular steatosis with retention of hepatic architecture.[53] PaDLOCs were treated with APAP and FIAU at 100 μM and 10 μM, respectively, before fixing and staining nuclei/cell regions and lipid droplets. Confocal images demonstrate that PaDLOCs treated with APAP resulted in a patchy loss of cell mask and shriveling of cells with no increased lipid accumulation as compared to control (Figure 3F). FIAU treated PaDLOCs however, showed high liquid accumulation and a reduction of CellMask staining suggestive of structural perturbation. Both PaDLOC observations for APAP and FIAU recapitulate the histological presentation and clinical phenotype of DILI in humans.

Modelling Hepatotoxicity of Inarigivir Combinations

The unexpected case of inarigivir soproxil-induced hepatotoxicity serves as a recent reminder of the need for improved pre-clinical assays for DILI risk assessment and serves as a suitable benchmark for both the 384-well HLO assay and the PaDLOC system. Cells in 384-well plates were treated with a 16-point dose range of tenofovir, TAF, inarigivir soproxil, and combinations thereof (tenofovir/inarigivr, and TAF/inarigivir). After 72 hrs of treatment, cells were stained to delineate nuclei/cell regions and to quantitate the mitochondrial, and lipid phenotypes. Confocal images were taken for each treatment condition (n = 4 wells). Morphological features for

bioRxiv preprint doi: https://doi.org/10.1101/2021.08.26.457824; this version posted August 28, 2021. The copyright holder for this preprint (which was not certified by peer review) is the author/funder, who has granted bioRxiv a license to display the preprint in perpetuity. It is made available under aCC-BY-NC-ND 4.0 International license.

each cell channel were obtained on a per-cell level along with reductions in cell count (a measure of cytotoxicity, cell death, and detachment). 100% loss of cell viability was observed in both drug combinations (Figure 4A, IC_{50} = 56.9 and 31.9 μM for tenofovir/inarigvir and TAF/inarigivir respectively) while negligible cytotoxicity was observed for the monotherapies up to concentrations of 100 μM. In addition to simple loss of cells, cytotoxicity was also measured by significant hepatocellular morphologic perturbation through multivariate analysis of cell features.[54] Random forest regression models between DMSO and FIAU treated controls were developed and used to score each cell on a predicted extent of FIAU exposure. These models were applied to all cells across all conditions, resulting in the ability to quantify hepatotoxicity through morphological features independent of cell count. Using this method, we observed minimal morphological perturbation of cells treated with either tenofovir variant individually as compared to DMSO-control with slight morphological perturbation for inarigivir treated cells. Morphologic perturbation analysis showed that both combinations resulted in pronounced cell morphologic perturbations like FIAU with IC_{50} of 21.4 and 41.6 μM for tenofovir and TAF respectively.

Tenofovir, tenofovir alafenamide (prodrug given in clinical trials), and inarigivir (500 nM) monotherapy all did not increase ALT or AST release after treatment and no morphological deviation from DMSO-treated control. However, the combination of tenofovir and inarigivir increased both ALT and AST starting at day 4 to an ALT level of 22 U/L, and further ALT increase to 33 U/L at 7 days of exposure and AST of 29 U/L and 45 U/L respectively (Figure 4B and C). TAF and inarigivir also resulted in ALT increase to 33 U/L at 7 days and AST to 42 U/L but did not show a significant increase at day 4. Both combination treatments also resulted in a decrease in albumin production while no effect was observed in the single-agent treatments across the 7 days (Figure 4D).

bioRxiv preprint doi: https://doi.org/10.1101/2021.08.26.457824; this version posted August 28, 2021. The copyright holder for this preprint (which was not certified by peer review) is the author/funder, who has granted bioRxiv a license to display the preprint in perpetuity. It is made available under aCC-BY-NC-ND 4.0 International license.

Visually (Figure 4F), PaDLOCs treated with both combinations exhibited a remarkably similar phenotype to FIAU-treated controls and dissimilar to the APAP control. To quantify observations from confocal microscopy, we employed a cell morphological profiling-based approach in the same manner as in the 384-HLO system. These measured features were reduced via UMAP into a 2-dimensional projection (Figure 4E) and tenofovir/inarigivir-treated cells clustered closely with that of FIAU treatment while tenofovir and inarigivir single-agent treatments clustered closely with DMSO control. APAP treated cells exhibited a phenotype unlike either of the other groups and resulted in their unique cluster suggesting that this system is capable of categorizing DILI by the mechanism of action by comparison to known controls.

Transcriptomic analysis of Tenofovir-Inarigivir, FIAU, APAP treated PaDLOCs

scRNAseq was performed on drug-treated and control PaDLOCs on the Illumina NovaSeq platform to suggest possible MOA of synergistic hepatotoxicity. The concentration and duration of treatment were optimized using phenotypic endpoints to capture intermediate phenotypes rather than late-stage cell death. DMSO-treated controls, fialuridine (1 μM), tenofovir (500 nM), and tenofovir/inarigivir (250 + 250 nM) combination were evaluated. Single-cell data was subset to the hepatocyte population based on known hepatocyte markers as listed in Figure 3G. Although phenotypically and clinically, tenofovir/inarigivir-induced hepatotoxicity shares similarities to that of fialuridine, our comparisons suggest a greater transcriptomic similarity between tenofovir monotherapy and fialuridine. First, UMAP re-embedding of the hepatocytes shows close clustering between fialuridine and tenofovir treatments. Volcano plots show that both conditions, compared to control, resulting in overexpression of KCNQ10T1 and NFIA, both related to gene expression regulation, and suppressed expression of RPS10.

Hepatocyte-specific differential expression analysis also suggests similar transcriptomic perturbation by fialuridine and tenofovir. Fatty acid, triglyceride, and lipid storage markers were of particular interest due to

bioRxiv preprint doi: https://doi.org/10.1101/2021.08.26.457824; this version posted August 28, 2021. The copyright holder for this preprint (which was not certified by peer review) is the author/funder, who has granted bioRxiv a license to display the preprint in perpetuity. It is made available under aCC-BY-NC-ND 4.0 International license.

observations through confocal microscopy. DGAT1, involved in triglyceride synthesis and storage[55], is downregulated under both fialuridine and tenofovir treatment when expression under tenofovir/inarigivir combination treatment matches that of vehicle control (Figure 5C). PLIN4, thought to aid in lipid droplet accumulation in the liver,[56] is not detected in the vehicle control but increased in all other conditions (Figure 5D). FABP4 is expressed consistently in all but the combination treatment (Figure 5E), conflicting with previous evidence that FABP4 is overexpressed in liver injury due to hepatocellular carcinoma .[57–59] However, other reports have shown that FABP4 knockdown results in greater adiposity in mice.[60]

Across all treatments, we observe diminishment of NDUFA4 as compared to control (Figure 5F) suggesting impairment to oxidative phosphorylation commonly associated with DILI.[61] We also observed decreased expression of PRDX4 in all treatments (Figure 5G), and GSTP1 in fialuridine and tenofovir single treatments (Figure 5H), indicators of oxidative stress.[62,63] Based on these observations, and since tenofovir monotherapy does not present as DILI, the synergistic toxicity of tenofovir/inarigivir is likely to be caused by misregulation of triglyceride synthesis and storage in addition to oxidative phosphorylation impairment and oxidative stress. These findings serve as a basis for future studies which are necessary to confirm the mechanism of action.

Discussion

We have established that HLOs are a viable *in vitro* model for DILI risk prediction and are amenable to high-throughput screening and adaptation to a liver-chip system that further enhances their organotypic function. They exhibit physiologic similarities to human liver including; 1) production of cell types from the same host genetics including hepatocyte-like cells, stellates and Kupffer cells, 2) albumin production, and 3) cytochrome P450 expression that makes them useful for modeling drug metabolism. HLOs have enabled large-scale and high throughput DILI risk assessment due to their relative scalability and consistency as compared to primary human hepatocytes. Their application in 384-well format can serve as the basis for an early-stage preclinical

bioRxiv preprint doi: https://doi.org/10.1101/2021.08.26.457824; this version posted August 28, 2021. The copyright holder for this preprint (which was not certified by peer review) is the author/funder, who has granted bioRxiv a license to display the preprint in perpetuity. It is made available under aCC-BY-NC-ND 4.0 International license.

assessment of novel molecular entities. In addition to detecting a reduction in viability upon drug treatment, multiplexed high-content screening and morphological cell profiling can give robust multivariate outputs that can be used to cluster drugs by their phenotypic fingerprint to impute similar mechanisms of action to known compounds. For example, FIAU treatment at sub-cytotoxic concentrations results in perturbation of cells that are similar to those observed clinically including diminished mitochondrial mass and lipid accumulation (Supplementary Figure 3). Many of these single-endpoints however are not independently robust and do not allow for reliable IC_{50} determination. Machine learning-based multivariate analysis, in this case, enabled through random forest regression against controls, bootstraps multiple single-endpoints to a robust DILI prediction score.

As we can generate iPSCs from patient PBMCs,[64] the 384-well format can be used to rapidly assess differential DILI risk per patient by screening a standard DILI drug library. Future studies will focus on developing a biobank of HLOs established from DILI patients thereby concentrating DILI genetics to a screenable number of patient lines that can be used as a predictive platform that can capture DILI risk with 10^6 enrichment over the general population. While high-throughput screening with dispersed HLOs in 384-well plates shows predictive power and can be used for large screening efforts, they suffer from lower CYP450 expression and lack of crucial hepatocyte function, both of which were mentioned as limitations in the original protocol for HLO culture.[13] While superior to hepatocellular carcinoma cell lines, the observed IC_{50} values for HLOs loss of cell viability are much higher than the achievable *in vivo* C_{max}. This is a limitation for preclinical assessment, as compounds appear less potent for producing DILI than *in vivo*, however, this may be compensated for through regression analysis.

Although PaDLOCs are less amenable to high-throughput screening of large small-molecule libraries, the enhancements in drug metabolism and hepatocyte function warrant its use in late-stage preclinical development

bioRxiv preprint doi: https://doi.org/10.1101/2021.08.26.457824; this version posted August 28, 2021. The copyright holder for this preprint (which was not certified by peer review) is the author/funder, who has granted bioRxiv a license to display the preprint in perpetuity. It is made available under aCC-BY-NC-ND 4.0 International license.

that does not necessitate high-throughput screening. The presence of CYP expression in PaDLOCs results in significant advantages for DILI risk prediction, as they can be used to observe effects of Phase 1/Phase 2 metabolites in addition to the parent compound. This is apparent in APAP-induced toxicity in PaDLOCs, as hepatotoxicity is only caused by metabolite NAPQI by CYP2E1 conversion.[65] Hepatotoxic concentrations in cancer cell systems for APAP are generally in the millimolar concentration range where general xenobiotic cytotoxicity and promiscuous binding interfere with general cell health,[66] whereas HLOs sufficiently predict DILI risk at 10^3 lower concentrations where mechanistic dissection is tractable. This model was also able to reliably predict hepatotoxicity as caused by both FIAU and the tenofovir/inarigivir combination, both of which were not made apparent until the treatments reached clinical trials and caused severe hepatotoxicity in human subjects.[7,67] Future efforts will also include building a diverse library of PaDLOCs from idiosyncratic DILI patients towards the development of a co-culture system with immune cells to capture inflammatory and auto-immune modulation of DILI. High-throughput screening can be performed on large drug screening libraries to tabulate DILI risk to help guide drug development and also to provide robust data sets to improve AI/ML computational prediction of DILI risk.

The integration of scRNAseq, shown here as a proof-of-concept for liver chip systems, can provide detailed single-cell transcriptomic data that can illuminate the mechanism of action. Herein, we present a unified multi-omics platform that delivers integrated biochemical endpoints (ALT/AST/Albumin/P450), high content imaging to robustly determine drug hepatocellular toxicity, morphologic cell profiling to generate single-cell phenotypic fingerprints in response to sub-toxic concentrations of drugs and single-cell transcriptomics to characterize significant phenotypic perturbations. This platform demonstrates significant advantages over conventional pre-clinical DILI models and can be used to de-risk novel molecular entities, potentially stratify DILI patients by

bioRxiv preprint doi: https://doi.org/10.1101/2021.08.26.457824; this version posted August 28, 2021. The copyright holder for this preprint (which was not certified by peer review) is the author/funder, who has granted bioRxiv a license to display the preprint in perpetuity. It is made available under aCC-BY-NC-ND 4.0 International license.

their drug responsiveness, and create model systems for distinct DILI subtypes for use in phenotypic drug discovery towards chemoprotective therapies.

Acknowledgements

Funding: JZS is supported by the National Institute of Diabetes and Digestive and Kidney Diseases (R01DK120623) and University of Michigan Institute for Clinical and Health Research (MICHR) (NCATS - UL1TR002240). CJZ is supported by a Rackham Merit Fellowship and SRM by pharmacological sciences training program (PSTP) T32 training grant. Transcriptomics was supported by the University of Michigan Center of Gastrointestinal Research (UMCGR) Single Cell Pilot Grant (5 P30 DK034933).

The authors would like to thank Emulate Inc. for assistance with experimental design. We thank Kevin Jan, Peyton Uhl, and Cassandra Rogers at Yokogawa for microscopy support. We also thank Teresa O'Meara for writing assistance and proofreading, and Carmen Mirabelli, Mack Reynolds, and Bishr Omary for thoughtful advice.

bioRxiv preprint doi: https://doi.org/10.1101/2021.08.26.457824; this version posted August 28, 2021. The copyright holder for this preprint (which was not certified by peer review) is the author/funder, who has granted bioRxiv a license to display the preprint in perpetuity. It is made available under aCC-BY-NC-ND 4.0 International license.

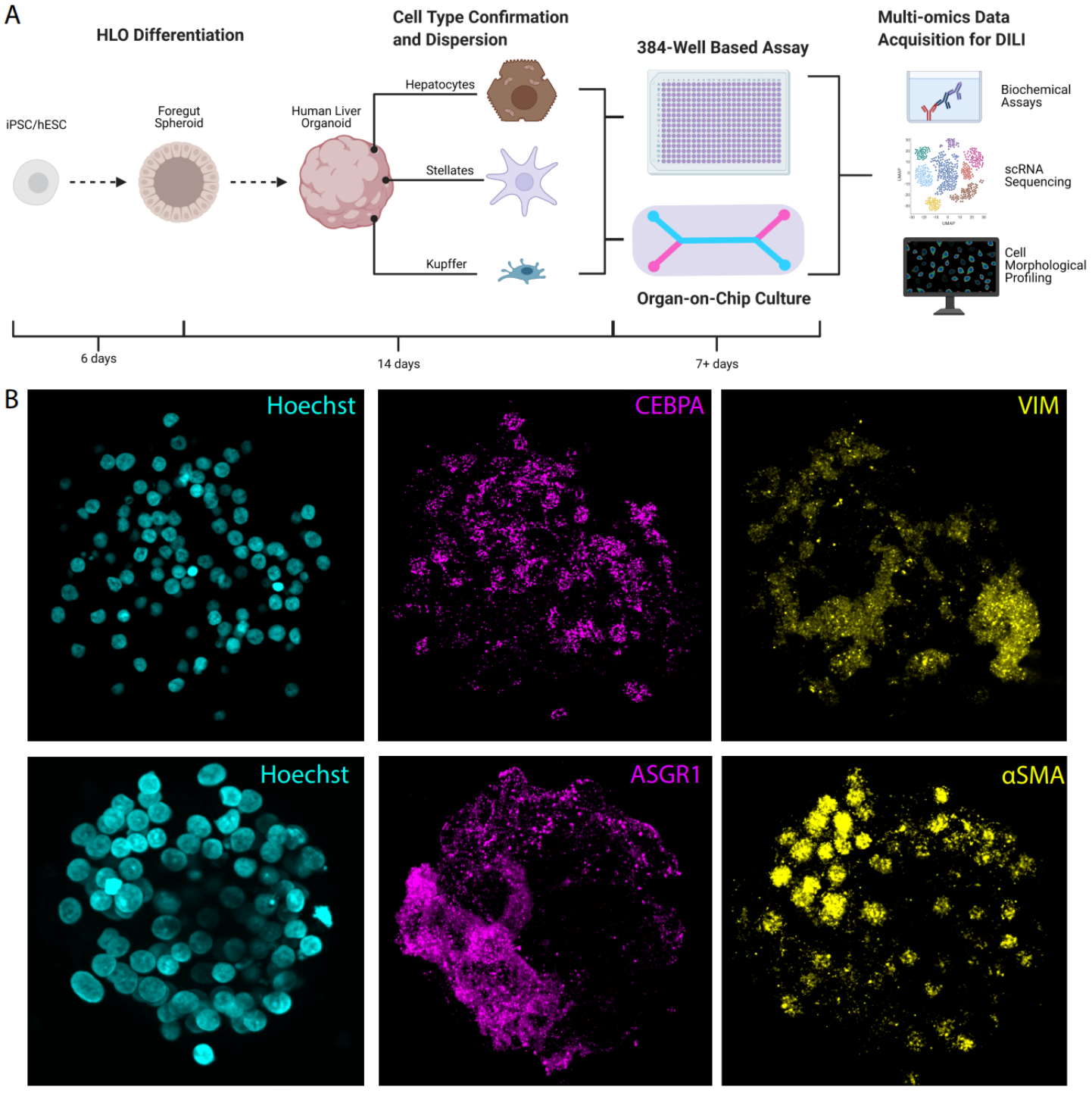

Figure 1. (A) Outline of the HLO differentiation process followed by disruption and dispersion of the organoid to plate in 384-well plates and a chip system for acquisition of biochemical, transcriptomic, and morphological

bioRxiv preprint doi: https://doi.org/10.1101/2021.08.26.457824; this version posted August 28, 2021. The copyright holder for this preprint (which was not certified by peer review) is the author/funder, who has granted bioRxiv a license to display the preprint in perpetuity. It is made available under aCC-BY-NC-ND 4.0 International license.

endpoints. (B) Confocal images of HLOs stained for nuclei, hepatocyte markers (CEBPA and HNF4A) and stellate markers (VIM and ACTA) for confirmation of the presence of cell types.

bioRxiv preprint doi: https://doi.org/10.1101/2021.08.26.457824; this version posted August 28, 2021. The copyright holder for this preprint (which was not certified by peer review) is the author/funder, who has granted bioRxiv a license to display the preprint in perpetuity. It is made available under aCC-BY-NC-ND 4.0 International license.

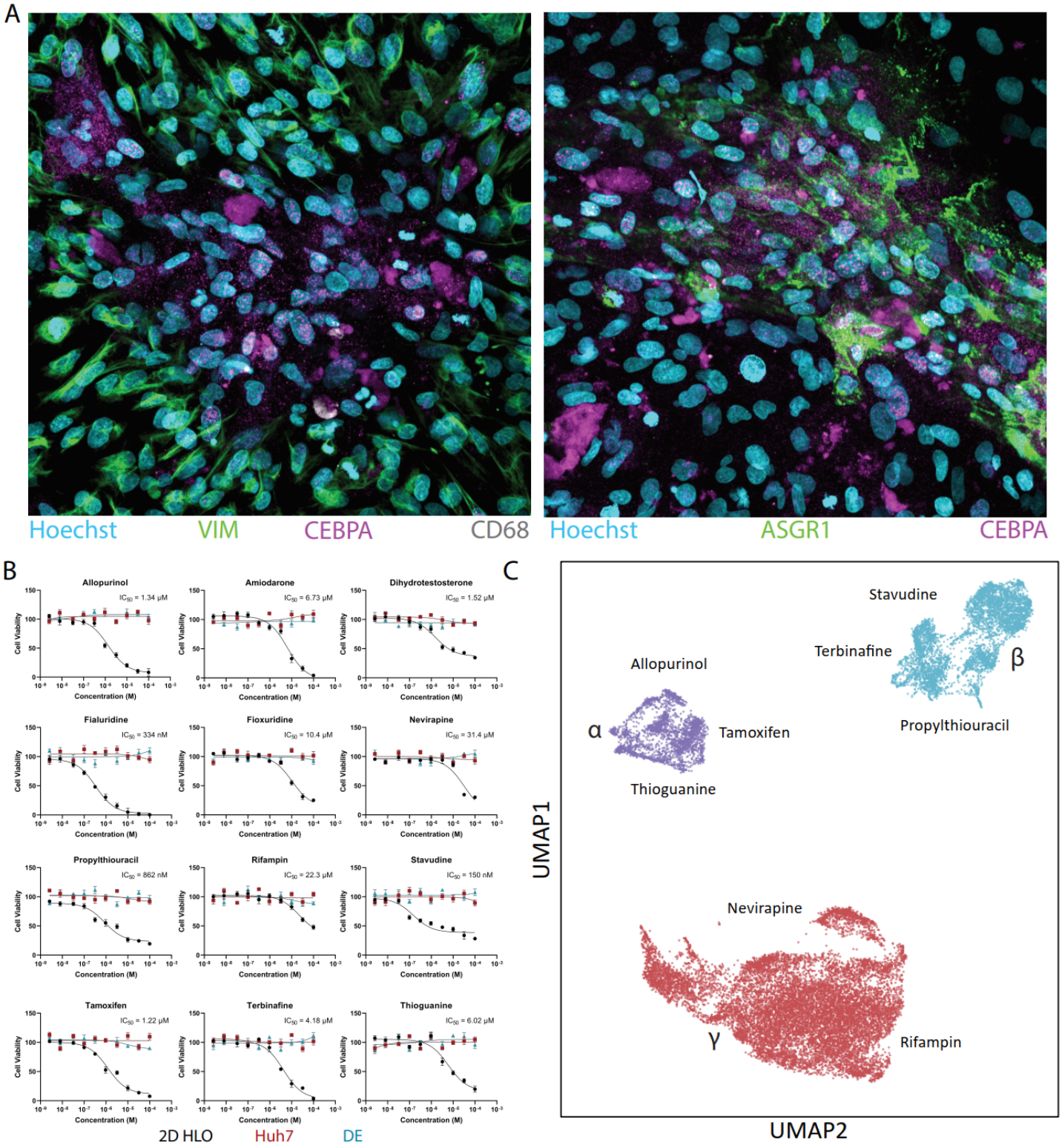

bioRxiv preprint doi: https://doi.org/10.1101/2021.08.26.457824; this version posted August 28, 2021. The copyright holder for this preprint (which was not certified by peer review) is the author/funder, who has granted bioRxiv a license to display the preprint in perpetuity. It is made available under aCC-BY-NC-ND 4.0 International license.

Figure 2. (A) HLOs disrupted and cultured in 384-well plates maintain expression of hepatocyte, stellate, and Kupffer cell markers. (B) Cell viability of 384-well cultures (black) treated with 12 known DILI-causing compounds in 10-point dose-response. Compounds were counter screened in immortalized cell line Huh7 (red) and definitive endoderm (blue) as controls. Plot points represent mean ± SD (n=4 per concentration, per cell line) (C) Cells treated at each compound's respective IC_{50} value stained with Hoechst 33342, MitoView Green, HCS CellMaskOrange, and LipidTox DeepRed were embedded into UMAP.

bioRxiv preprint doi: https://doi.org/10.1101/2021.08.26.457824; this version posted August 28, 2021. The copyright holder for this preprint (which was not certified by peer review) is the author/funder, who has granted bioRxiv a license to display the preprint in perpetuity. It is made available under aCC-BY-NC-ND 4.0 International license.

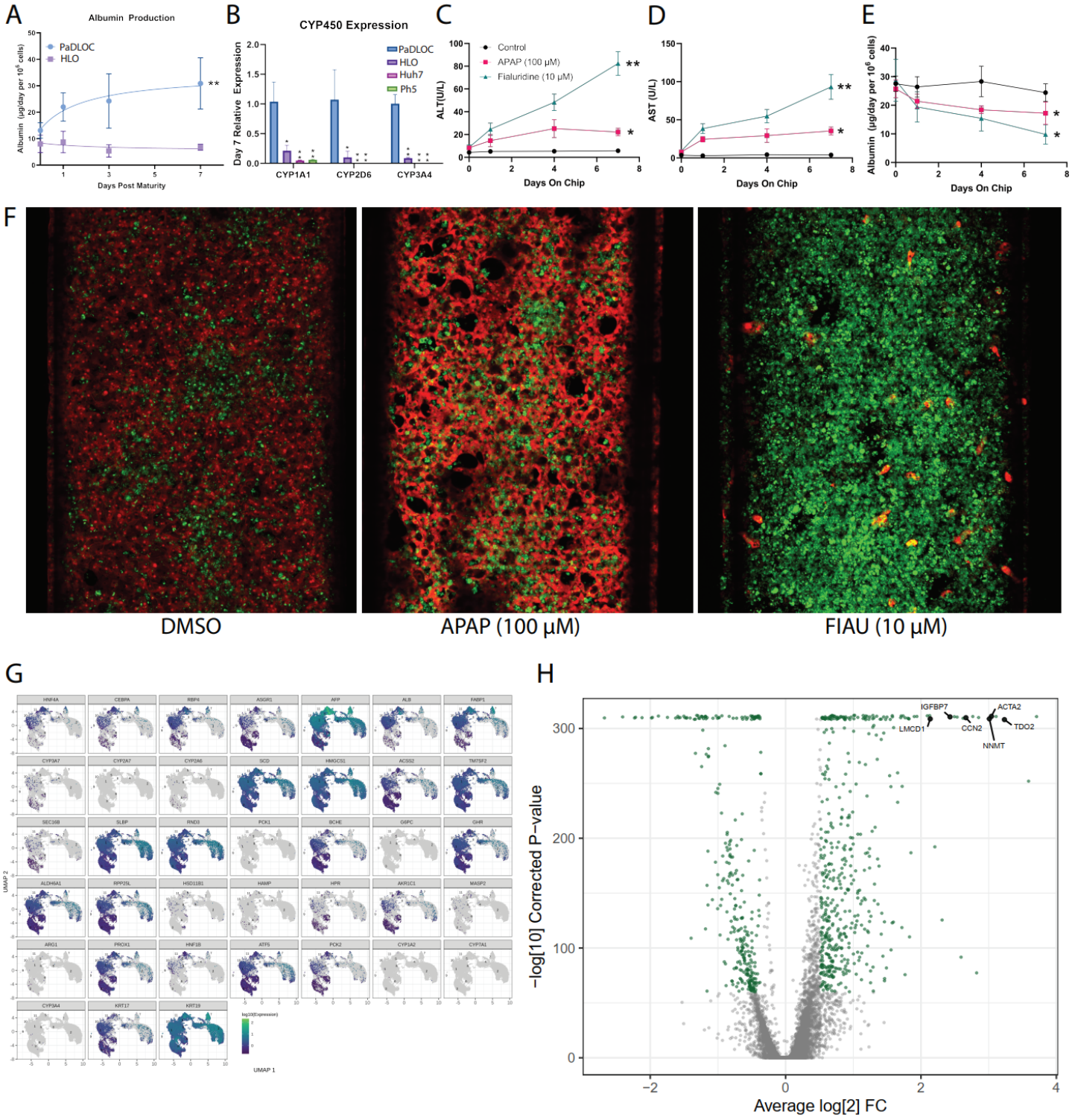

451

bioRxiv preprint doi: https://doi.org/10.1101/2021.08.26.457824; this version posted August 28, 2021. The copyright holder for this preprint (which was not certified by peer review) is the author/funder, who has granted bioRxiv a license to display the preprint in perpetuity. It is made available under aCC-BY-NC-ND 4.0 International license.

Figure 3. HLOs are disrupted into single-cell suspension and cultured on the Emulate Bio Chip-S1 for 7 days. (A) Albumin released in PaDLOCs is identical to that of intact HLOs at day 0 but increases over 7 days (day 21-28 of differentiation). (B) Relative expression of select CYP450s between PaDLOCs, intact HLO, and immortalized hepatocyte cell lines Huh7 and Ph5. (C) Cells are treated with DMSO control and known hepatotoxins APAP (100 μM) and FIAU (1 μM). PaDLOCs demonstrated both ALT (D) and AST release and (E) albumin production diminishment across 7 days. (F) Confocal images of PaDLOCs at day 7 of treatment stained with CellMask Orange (shown in red) and LipidTOX Deep Red (colored green). Bars and plot points represent mean ± SD (n=3 PaDLOC chips and n=3 intact HLO wells). (G) UMAP embedding of PaDLOCs with highlighted hepatocyte markers. (H) Volcano plot comparing gene differential expression between PaDLOC and HLOs with genes most upregulated in PaDLOC highlighted.

bioRxiv preprint doi: https://doi.org/10.1101/2021.08.26.457824; this version posted August 28, 2021. The copyright holder for this preprint (which was not certified by peer review) is the author/funder, who has granted bioRxiv a license to display the preprint in perpetuity. It is made available under aCC-BY-NC-ND 4.0 International license.

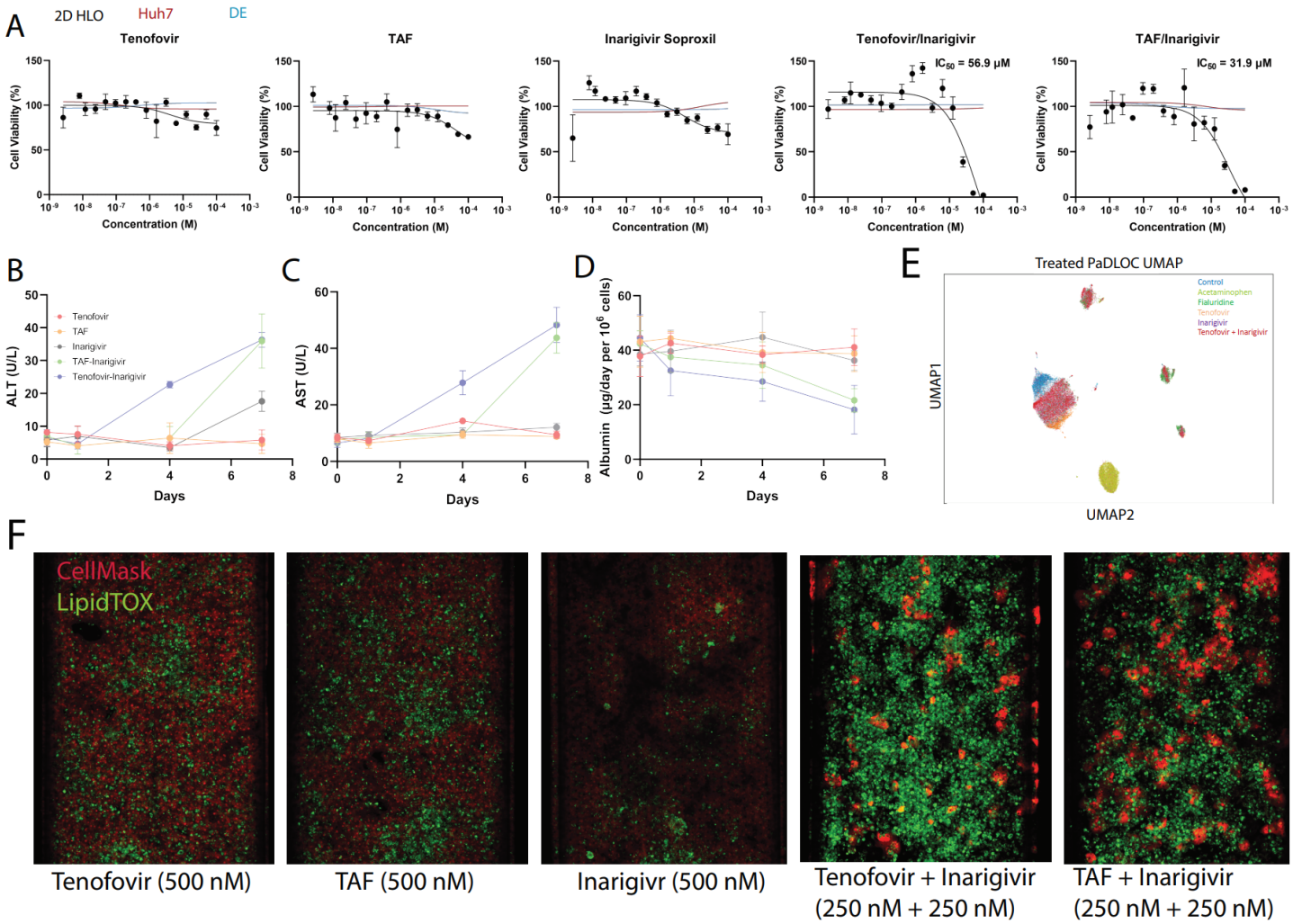

Figure 4. (A) Cell viability of 2D 384-well monolayer cultures of dispersed HLOs treated in 16-point dose-response with tenofovir, TAF, or inarigivir soproxil (n=4 per concentration) and measured IC_{50}. (B) ALT, (C) AST, (D) and albumin released by PaDLOCs over 7 days of treatment with tenofovir (500 nM), TAF (500 nM), inarigivir soproxil (500 nM), tenofovir-inarigivir combination (250-250 nM), and TAF-inarigivir combination (250-250 nM) (n=3 chips per condition). Plot points represent mean ± SD. (E) PaDLOCs treated with DMSO control, individual agents, combinations, APAP, and FIAU were stained with Hoechst 33342, CellMask Orange, and LipidTOX Deep Red. CellProfiler 4.2.0 was used to extract cell-level features to embed into UMAP. (F) Representative images of treated PaDLOCs.

bioRxiv preprint doi: https://doi.org/10.1101/2021.08.26.457824; this version posted August 28, 2021. The copyright holder for this preprint (which was not certified by peer review) is the author/funder, who has granted bioRxiv a license to display the preprint in perpetuity. It is made available under aCC-BY-NC-ND 4.0 International license.

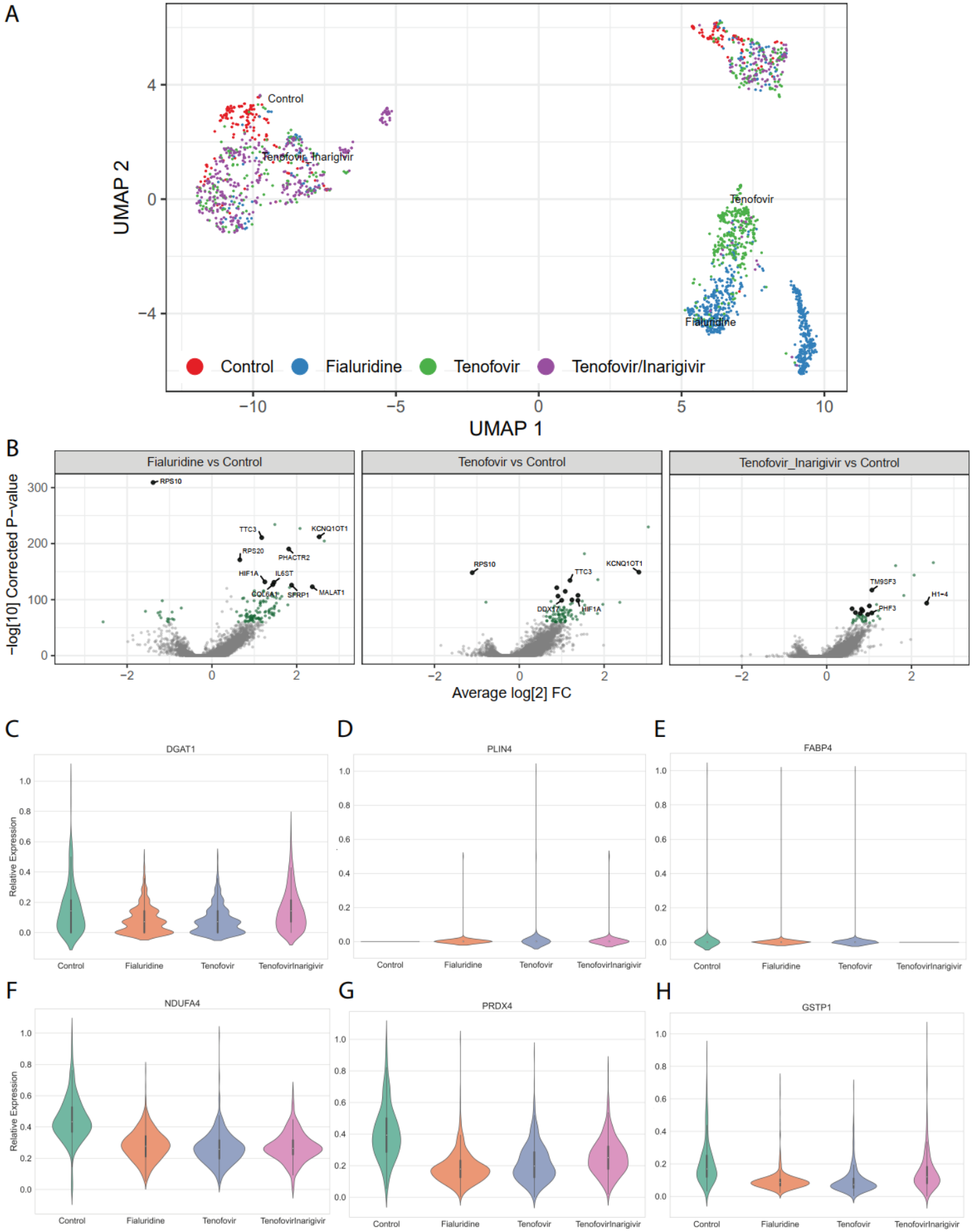

bioRxiv preprint doi: https://doi.org/10.1101/2021.08.26.457824; this version posted August 28, 2021. The copyright holder for this preprint (which was not certified by peer review) is the author/funder, who has granted bioRxiv a license to display the preprint in perpetuity. It is made available under aCC-BY-NC-ND 4.0 International license.

Figure 5. (A) Hepatocytes across treatments are identified and subset through marker expression and embedded into a UMAP to visualize similarities between treatments. (B) Volcano plots highlighting significant differential expression between control and drug treatments (>0 designates higher expression in treatment). (C-H) Relative expression of genes in vehicle control, fialuridine, tenofovir, and tenofovir-inarigivir treated PaDLOCs.

References

1. Fontana RJ, Watkins PB, Bonkovsky HL, et al. Drug-Induced Liver Injury Network (DILIN) prospective study: rationale, design and conduct. Drug Saf 2009;32:55–68.

2. Fontana RJ, Seeff LB, Andrade RJ, et al. Standardization of nomenclature and causality assessment in drug-induced liver injury: summary of a clinical research workshop. Hepatology 2010;52:730–742.

3. Bakke OM, Manocchia M, Abajo F de, et al. Drug safety discontinuations in the United Kingdom, the United States, and Spain from 1974 through 1993: a regulatory perspective. Clin Pharmacol Ther 1995;58:108–117.

4. Watkins PB. Drug safety sciences and the bottleneck in drug development. Clin Pharmacol Ther 2011;89:788–790.

5. Gindi R, National Center for Health Statistics (U.S.). Health, United States, 2019. 2021. Available at: http://dx.doi.org/10.15620/cdc:100685.

6. Yuen M-F, Elkashab M, Chen C-Y, et al. Dose response and safety of the daily, oral RIG-I agonist Inarigivir (SB 9200) in treatment naïve patients with chronic hepatitis B: results from the 25mg and 50mg cohorts in the ACHIEVE trial. Journal of Hepatology 2018;68:S509–S510. Available at: http://dx.doi.org/10.1016/s0168-8278(18)31267-4.

7. Kosh Agarwal, Nezam Afdhal, Carla Coffin, Scott Fung, Geoffrey Dusheiko, Graham Foster, Magdy Elkhashab, Edward Tam, Alnoor Ramji, Radhakrishnan Iyer, Patrick Kennedy. Liver toxicity in the Phase 2 Catalyst 206 trial of inarigivir 400mg daily added to a nucleos(t)ide in HBeAg negative patients. 2020.

8. Gomez-Lechon MJ, Donato MT, Lahoz A, et al. Cell Lines: A Tool for In Vitro Drug Metabolism Studies. Curr Drug Metab 2008;9:1–11.

9. Jeffries RE, Gamcsik MP, Keshari KR, et al. Effect of Oxygen Concentration on Viability and Metabolism in a Fluidized-Bed Bioartificial Liver Using 31P and 13C NMR Spectroscopy. Tissue Eng

bioRxiv preprint doi: https://doi.org/10.1101/2021.08.26.457824; this version posted August 28, 2021. The copyright holder for this preprint (which was not certified by peer review) is the author/funder, who has granted bioRxiv a license to display the preprint in perpetuity. It is made available under aCC-BY-NC-ND 4.0 International license.

Part C Methods 2013;19:93–100.

10. Stéphenne X, Najimi M, Sokal EM. Hepatocyte cryopreservation: is it time to change the strategy? World J Gastroenterol 2010;16:1–14.

11. Olson H, Betton G, Robinson D, et al. Concordance of the toxicity of pharmaceuticals in humans and in animals. Regul Toxicol Pharmacol 2000;32:56–67.

12. Jang K-J, Otieno MA, Ronxhi J, et al. Reproducing human and cross-species drug toxicities using a Liver-Chip. Sci Transl Med 2019;11. Available at: http://dx.doi.org/10.1126/scitranslmed.aax5516.

13. Thompson WL, Takebe T. Generation of multi-cellular human liver organoids from pluripotent stem cells. Methods Cell Biol 2020;159:47–68.

14. Ouchi R, Togo S, Kimura M, et al. Modeling Steatohepatitis in Humans with Pluripotent Stem Cell-Derived Organoids. Cell Metab 2019;30:374–384.e6.

15. Sheyn D, Cohn-Yakubovich D, Ben-David S, et al. Bone-chip system to monitor osteogenic differentiation using optical imaging. Microfluid Nanofluidics 2019;23. Available at: http://dx.doi.org/10.1007/s10404-019-2261-7.

16. McCracken KW, Catá EM, Crawford CM, et al. Modelling human development and disease in pluripotent stem-cell-derived gastric organoids. Nature 2014;516:400–404.

17. Sugawara S, Ito T, Sato S, et al. Production of an aminoterminally truncated, stable type of bioactive mouse fibroblast growth factor 4 in Escherichia coli. J Biosci Bioeng 2014;117:525–530.

18. Anon. *Liver-Chip Co-Culture Protocol*. Emulate Inc.; 2019. Available at: https://emulatebio.com/wp-content/uploads/2021/06/EP008_v5.0_Liver-Chip_Co-Culture_Protocol.pdf.

19. Frankish A, Diekhans M, Ferreira A-M, et al. GENCODE reference annotation for the human and mouse genomes. Nucleic Acids Res 2019;47:D766–D773.

20. Zheng GXY, Terry JM, Belgrader P, et al. Massively parallel digital transcriptional profiling of single cells. Nat Commun 2017;8:14049.

21. Duncan AW, Taylor MH, Hickey RD, et al. The ploidy conveyor of mature hepatocytes as a source of genetic variation. Nature 2010;467:707–710.

22. Choudhary S, Satija R. Comparison and evaluation of statistical error models for scRNA-seq. bioRxiv 2021. Available at: https://www.biorxiv.org/content/10.1101/2021.07.07.451498.abstract.

23. Hao Y, Hao S, Andersen-Nissen E, et al. Integrated analysis of multimodal single-cell data. Cell 2021;184:3573–3587.e29.

24. Love MI, Huber W, Anders S. Moderated estimation of fold change and dispersion for RNA-seq data with DESeq2. Genome Biol 2014;15:550.

bioRxiv preprint doi: https://doi.org/10.1101/2021.08.26.457824; this version posted August 28, 2021. The copyright holder for this preprint (which was not certified by peer review) is the author/funder, who has granted bioRxiv a license to display the preprint in perpetuity. It is made available under aCC-BY-NC-ND 4.0 International license.

25. McInnes L, Healy J, Melville J. UMAP: Uniform Manifold Approximation and Projection for Dimension Reduction. arXiv [statML] 2018. Available at: http://arxiv.org/abs/1802.03426.

26. Cao J, Spielmann M, Qiu X, et al. The single-cell transcriptional landscape of mammalian organogenesis. Nature 2019;566:496–502.

27. Melville J, Lun A, Djekidel MN. uwot: The uniform manifold approximation and projection (UMAP) method for dimensionality reduction. R package version 2020;15.

28. Traag VA, Waltman L, Eck NJ van. From Louvain to Leiden: guaranteeing well-connected communities. Sci Rep 2019;9:5233.

29. Becht E, McInnes L, Healy J, et al. Dimensionality reduction for visualizing single-cell data using UMAP. Nat Biotechnol 2018. Available at: http://dx.doi.org/10.1038/nbt.4314.

30. Berthold MR, Cebron N, Dill F, et al. KNIME: The Konstanz Information Miner. In: *Studies in Classification, Data Analysis, and Knowledge Organization (GfKL 2007)*. Springer; 2007.

31. Anon. How to use the Random Forest nodes. knime.com 2020. Available at: https://hub.knime.com/knime/spaces/Examples/latest/04_Analytics%2F13_Meta_Learning%2F02_Learning_a_Random_Forest~Sim-pKlioDWrgj_T [Accessed September 1, 2020].

32. McCracken KW, Howell JC, Wells JM, et al. Generating human intestinal tissue from pluripotent stem cells in vitro. Nat Protoc 2011;6:1920–1928.

33. Knolle P, Löhr H, Treichel U, et al. Parenchymal and nonparenchymal liver cells and their interaction in the local immune response. Z Gastroenterol 1995;33:613–620.

34. Fausther M, Pritchard MT, Popov YV, et al. Contribution of Liver Nonparenchymal Cells to Hepatic Fibrosis: Interactions with the Local Microenvironment. BioMed Research International 2017;2017:1–4. Available at: http://dx.doi.org/10.1155/2017/6824762.

35. Shinozawa T, Kimura M, Cai Y, et al. High-Fidelity Drug-Induced Liver Injury Screen Using Human Pluripotent Stem Cell–Derived Organoids. Gastroenterology 2021;160:831–846.e10.

36. Haney SA. *High Content Screening: Science, Techniques and Applications*. John Wiley & Sons; 2008.

37. Mirabelli C, Wotring JW, Zhang CJ, et al. Morphological cell profiling of SARS-CoV-2 infection identifies drug repurposing candidates for COVID-19. bioRxivorg 2020. Available at: http://biorxiv.org/lookup/doi/10.1101/2020.05.27.117184.

38. Carpenter AE, Jones TR, Lamprecht MR, et al. CellProfiler: image analysis software for identifying and quantifying cell phenotypes. Genome Biol 2006;7:R100.

39. McInnes L, Healy J, Astels S. hdbscan: Hierarchical density based clustering. J Open Source Softw 2017;2:205.

bioRxiv preprint doi: https://doi.org/10.1101/2021.08.26.457824; this version posted August 28, 2021. The copyright holder for this preprint (which was not certified by peer review) is the author/funder, who has granted bioRxiv a license to display the preprint in perpetuity. It is made available under aCC-BY-NC-ND 4.0 International license.

40. Dickson I. Multispecies liver-on-a-chip for improved drug toxicity testing. Nat Rev Gastroenterol Hepatol 2020;17:4.

41. Rachfal AW, Brigstock DR. Connective tissue growth factor (CTGF/CCN2) in hepatic fibrosis. Hepatol Res 2003;26:1–9.

42. Goulart E, Caires-Junior LC de, Telles-Silva KA, et al. Adult and iPS-derived non-parenchymal cells regulate liver organoid development through differential modulation of Wnt and TGF-β. Stem Cell Res Ther 2019;10:258.

43. Rodansky ES, Johnson LA, Huang S, et al. Intestinal organoids: a model of intestinal fibrosis for evaluating anti-fibrotic drugs. Exp Mol Pathol 2015;98:346–351.

44. Ding Q, Ma Y, Lai S, et al. NNMT aggravates hepatic steatosis, but alleviates liver injury in alcoholic liver disease. J Hepatol 2021;74:1248–1250.

45. Allard JB, Duan C. IGF-Binding Proteins: Why Do They Exist and Why Are There So Many? Front Endocrinol 2018;9:117.

46. McGill MR. The past and present of serum aminotransferases and the future of liver injury biomarkers. EXCLI J 2016;15:817–828.

47. European Association for the Study of the Liver. Electronic address: easloffice@easloffice.eu, Clinical Practice Guideline Panel: Chair:, Panel members, et al. EASL Clinical Practice Guidelines: Drug-induced liver injury. J Hepatol 2019;70:1222–1261.

48. James LP, Letzig L, Simpson PM, et al. Pharmacokinetics of acetaminophen-protein adducts in adults with acetaminophen overdose and acute liver failure. Drug Metab Dispos 2009;37:1779–1784.

49. Dahlin DC, Miwa GT, Lu AY, et al. N-acetyl-p-benzoquinone imine: a cytochrome P-450-mediated oxidation product of acetaminophen. Proc Natl Acad Sci U S A 1984;81:1327–1331.

50. Honkoop P, Scholte HR, Man RA de, et al. Mitochondrial Injury Lessons from the Fialuridine Trial. Drug Safety 1997;17:1–7. Available at: http://dx.doi.org/10.2165/00002018-199717010-00001.

51. Krähenbühl S. Mitochondria: important target for drug toxicity? J Hepatol 2001;34:334–336.

52. Hinson JA, Roberts DW, James LP. Mechanisms of acetaminophen-induced liver necrosis. Handb Exp Pharmacol 2010:369–405.

53. Kleiner DE. Drug-induced liver injury: The hepatic pathologist's approach. Gastroenterol Clin North Am 2017;46:273–296.

54. Jones TR, Carpenter AE, Lamprecht MR, et al. Scoring diverse cellular morphologies in image-based screens with iterative feedback and machine learning. Proc Natl Acad Sci U S A 2009;106:1826–1831.

bioRxiv preprint doi: https://doi.org/10.1101/2021.08.26.457824; this version posted August 28, 2021. The copyright holder for this preprint (which was not certified by peer review) is the author/funder, who has granted bioRxiv a license to display the preprint in perpetuity. It is made available under aCC-BY-NC-ND 4.0 International license.

55. Villanueva CJ, Monetti M, Shih M, et al. Specific role for acyl CoA:Diacylglycerol acyltransferase 1 (Dgat1) in hepatic steatosis due to exogenous fatty acids. Hepatology 2009;50:434–442.

56. Griffin JD, Salter DM, Bowman T, et al. Role of Hepatic PLIN2 and PLIN4 in The Development of Western Type Diet Induced Hepatosteatosis. The FASEB Journal 2017;31:458.3–458.3.

57. Chiyonobu N, Shimada S, Akiyama Y, et al. Fatty Acid Binding Protein 4 (FABP4) Overexpression in Intratumoral Hepatic Stellate Cells within Hepatocellular Carcinoma with Metabolic Risk Factors. The American Journal of Pathology 2018;188:1213–1224. Available at: http://dx.doi.org/10.1016/j.ajpath.2018.01.012.

58. Thompson KJ, Austin RG, Nazari SS, et al. Altered fatty acid-binding protein 4 (FABP4) expression and function in human and animal models of hepatocellular carcinoma. Liver Int 2018;38:1074–1083.

59. Laouirem S, Sannier A, Norkowski E, et al. Endothelial fatty liver binding protein 4: a new targetable mediator in hepatocellular carcinoma related to metabolic syndrome. Oncogene 2019;38:3033–3046.

60. Yang R, Castriota G, Chen Y, et al. RNAi-mediated germline knockdown of FABP4 increases body weight but does not improve the deranged nutrient metabolism of diet-induced obese mice. Int J Obes 2011;35:217–225.

61. Pessayre D, Fromenty B, Berson A, et al. Central role of mitochondria in drug-induced liver injury. Drug Metab Rev 2012;44:34–87.

62. Yamada S, Guo X. Peroxiredoxin 4 (PRDX4): Its critical in vivo roles in animal models of metabolic syndrome ranging from atherosclerosis to nonalcoholic fatty liver disease. Pathology International 2018;68:91–101. Available at: http://dx.doi.org/10.1111/pin.12634.

63. Li T, Zhao X-P, Wang L-Y, et al. Glutathione S-transferase P1 correlated with oxidative stress in hepatocellular carcinoma. Int J Med Sci 2013;10:683–690.

64. Yu J, Vodyanik MA, Smuga-Otto K, et al. Induced pluripotent stem cell lines derived from human somatic cells. Science 2007;318:1917–1920.

65. Lee SST, Buters JTM, Pineau T, et al. Role of CYP2E1 in the Hepatotoxicity of Acetaminophen. Journal of Biological Chemistry 1996;271:12063–12067. Available at: http://dx.doi.org/10.1074/jbc.271.20.12063.

66. Nelson LJ, Navarro M, Treskes P, et al. Acetaminophen cytotoxicity is ameliorated in a human liver organotypic co-culture model. Sci Rep 2015;5:17455.

67. McKenzie R, Fried MW, Sallie R, et al. Hepatic failure and lactic acidosis due to fialuridine (FIAU), an investigational nucleoside analogue for chronic hepatitis B. N Engl J Med 1995;333:1099–1105.

bioRxiv preprint doi: https://doi.org/10.1101/2021.08.26.457824; this version posted August 28, 2021. The copyright holder for this preprint (which was not certified by peer review) is the author/funder, who has granted bioRxiv a license to display the preprint in perpetuity. It is made available under aCC-BY-NC-ND 4.0 International license.

633 68. Dekkers JF, Alieva M, Wellens LM, et al. High-resolution 3D imaging of fixed and cleared
634 organoids. Nat Protoc 2019;14:1756–1771.